RSC Advances

PAPER

View Article Online
View Journal | View Issue

Check for updates

Cite this: *RSC Adv.*, 2020, **10**, 40442

Suppressing loss tangent with significantly enhanced dielectric permittivity of poly(vinylidene fluoride) by filling with Au–$Na_{1/2}Y_{1/2}Cu_3Ti_4O_{12}$ hybrid particles

Pornsawan Kum-onsa,[a] Nutthakritta Phromviyo[b] and Prasit Thongbai *[cd]

Three-phase gold nanoparticle–$Na_{1/2}Y_{1/2}Cu_3Ti_4O_{12}$ (Au–NYCTO)/poly(vinylidene fluoride) (PVDF) composites with 0.095–0.487 hybrid particle volume fractions (f) were fabricated. Au nanoparticles with a diameter of ~10 nm were decorated on the surfaces of high-permittivity NYCTO particles using a modified Turkevich's method. The polar β-PVDF phase was confirmed to exist in the composites. Significantly enhanced dielectric permittivity of ~98 (at 1 kHz) was obtained in the Au–NYCTO/PVDF composite with $f_{Au-NYCTO} = 0.487$, while the loss tangent was suppressed to 0.09. Abrupt changes in the dielectric and electrical properties, which signified percolation behavior, were not observed even when $f_{Au-NYCTO} = 0.487$. Using the effective medium percolation theory model, the percolation threshold (f_c) was predicted to be at $f_{Au-NYCTO} = 0.69$, at which f_{Au} was estimated to ~0.19 and close to the theoretical f_c value for the conductor–insulator composites ($f_c = 0.16$). A largely enhanced dielectric response in the Au–NYCTO/PVDF composites was contributed by the interfacial polarization effect and a high permittivity of the NYCTO ceramic filler. Au nanoparticles can produce the local electric field in the composites, making the dipole moments in the β-PVDF phase and NYCTO particles align with the direction of the electric field.

Received 13th August 2020
Accepted 1st November 2020

DOI: 10.1039/d0ra06980a

rsc.li/rsc-advances

Open Access Article. Published on 06 November 2020. Downloaded on 12/5/2025 4:44:41 AM.
This article is licensed under a Creative Commons Attribution-NonCommercial 3.0 Unported Licence.

1. Introduction

Polymer-matrix composites (PMCs) with excellent dielectric properties are increasingly needed due to the rapid development of polymer-based electronics, especially energy-storage devices and embedded capacitors in microelectronics.[1–3] Basically, the process of improving the dielectric properties of PMCs must consist of several improvement procedures: (1) selection of polymer matrices that possess good dielectric properties, (2) selection of a ceramic filler with high dielectric permittivity, and/or (3) incorporation of a conductive organic or inorganic filler for incorporation into a polymer matrix.[4]

Poly(vinylidene fluoride) (PVDF) is an interesting polymer that has been widely used as a polymer matrix since it can exhibit a higher dielectric permittivity ($\varepsilon' \sim 10$) compared to other polymers.[5–7] Furthermore, PVDF has a high breakdown voltage, which is desirable for electronics applications.

High permittivity oxide particles (*e.g.*, $BaTiO_3$ (BT))[5,8,9] and giant permittivity oxides in the $ACu_3Ti_4O_{12}$ (*A*CTO) family[10–12] have been used as fillers in polymer matrices to enhance the dielectric permittivity (ε') of the PMCs. In addition to the $CaCu_3Ti_4O_{12}$ (CCTO) ceramic, the giant dielectric properties of other compounds in the *A*CTO family have been studied. Among them, $Na_{1/2}Y_{1/2}Cu_3Ti_4O_{12}$ (NYCTO) is one of the most interesting oxides that has been investigated.[13–15] NYCTO ceramics exhibited a large ε' values of ~10^3 to 10^4 with low loss tangents (tan δ) of ~0.03–0.1 at 1 kHz. Use of metallic fillers (*e.g.*, Ni,[16] Al,[17] and Ag[18,19]) is also a good strategy to achieve a high ε' value of metal–polymer composites with a relatively low loading. Unfortunately, it is hard to control the filler loading near the percolation threshold, which leads to a high tan δ as well.

Balancing the tradeoff between significantly increased ε' values while retaining low tan δ is still a challenge. In recent years, simultaneous incorporation of high-permittivity oxide particles and metallic nanoparticles have been used to prepare three-phase PMCs. This has become an effective way to obtain high ε' and simultaneously suppress the tan δ. The strategy of incorporating hybrid particles consisting of two different filler types into a polymer matrix is of great interest to researchers.

[a]*Materials Science and Nanotechnology Program, Faculty of Science, Khon Kaen University, Khon Kaen 40002, Thailand*
[b]*Sustainable Infrastructure Research and Development Center, Department of Civil Engineering, Faculty of Engineering, Khon Kaen University, Khon Kaen 40002, Thailand*
[c]*Department of Physics, Faculty of Science, Khon Kaen University, Khon Kaen 40002, Thailand. E-mail: pthongbai@kku.ac.th*
[d]*Institute of Nanomaterials Research and Innovation for Energy (IN–RIE), NANOTEC–KKU RNN on Nanomaterials Research and Innovation for Energy, Khon Kaen University, Khon Kaen 40002, Thailand*

This journal is © The Royal Society of Chemistry 2020

Open Access Article. Published on 06 November 2020. Downloaded on 12/5/2025 4:44:41 AM.
This article is licensed under a Creative Commons Attribution-NonCommercial 3.0 Unported Licence.

For example, Luo *et al.* found high a $\varepsilon' \sim 160$ and tan $\delta \sim 0.11$ (at 1 kHz) were obtained in PVDF matrix nanocomposites filled with Ag–BT hybrid nanoparticles.[20] Hybrid particles consisting of Au metal and NYCTO oxide nanoparticles may be one of the most effective fillers to obtain a PMC with high dielectric performance. To the best of our knowledge, a three-phase Au–NYCTO/PVDF composite system has never been reported.

In this work, a novel ternary phase composite employing Au and NYCTO as filler particles was fabricated in a PVDF polymer matrix. The NYCTO particles were synthesized *via* a combustion method. The surfaces of NYCTO particles were decorated with spherical Au nanoparticles using a modified Turkevich's method. Interestingly, a significantly enhanced dielectric response and low dielectric loss were accomplished in the resulting Au–NYCTO/PVDF composites. The dielectric behavior of the PMCs is described in detail.

2. Method

2.1 Preparation of NYCTO particles

NYCTO particles were synthesized using a combustion method. First, the appropriate amounts of $NaNO_3$ (99%, KANTO), $Y(NO_3)_3 \cdot 6H_2O$ (99.9%, KANTO) and $Cu(NO_3)_2 \cdot 4H_2O$ (99.5%, CARLO ERBA) were dissolved in CH_3COOH (ACI Labscan) using a magnetic bar stirrer at room temperature for 1 h to produce a homogenous solution. Then, $C_{16}H_{28}O_6Ti$ (75 wt%, Sigma-Aldrich) was dissolved into the solution and stirred for 1 h to obtain a transparent solution. Next, NH_2CH_2COOH (99%, ACI Labscan) was added into the solution and heated to 150 °C under continuous stirring to form a wet gel. After that, the gel was combusted at 350 °C for 0.5 h. Finally, a fine NYCTO powder was achieved by calcination at 1000 °C for 10 h.

2.2 Preparation of Au–NYCTO particles

Au–NYCTO hybrid particles were fabricated using a modified Turkevich's method. First, the obtained NYCTO particles were dispersed in deionized water with the aid of ultrasonication for 0.5 h. Next, this NYCTO solution was stirred for 0.5 h at room temperature. After that, 1 mM of $HAuCl_4 \cdot 3H_2O$ was dissolved in this solution and then temperature of solution was increased to 100 °C with constant stirring. Next, $C_6H_5Na_3O_7 \cdot 2H_2O$ (Sigma-Aldrich) was continuously dropped into the solution. To ensure the reaction was completed, the light brown solution was stirred until a dark brown solution was formed. After that, the dark brown solution was centrifuged at 8500 rpm and was washed several times with deionized water. Finally, the resulting powder was freeze-dried to produce Au–NYCTO particles.

2.3 Preparation of Au–NYCTO/PVDF polymer composites

Three-phase PMCs with various volume fractions of Au–NYCTO hybrid particles ($f_{Au-NYCTO}$) were prepared using the following steps. First, the Au–NYCTO hybrid particles were mixed with PVDF powder ($M_w \sim 534\,000$, Sigma-Aldrich) in ethanol by ball-milling for 3 h at room temperature. Then, the mixture was heated at 80 °C for 24 h to eliminate the ethanol. Next, the dried mixture of powders was molded to disk-shapes with a diameter of 12 mm and 1.0 mm in thickness under a pressure of 10 MPa and simultaneously heated to 200 °C for 0.5 h. Finally, Au–NYCTO/PVDF samples with $f_{Au-NYCTO} = 0$, 0.095, 0.191, 0.289, 0.387, and 0.487 were obtained and immediately cooled to room temperature. These Au–NYCTO/PVDF polymer composites are respectively referred to as the PVDF, Au–NYCTO/PVDF-1, Au–NYCTO/PVDF-2, Au–NYCTO/PVDF-3, Au–NYCTO/PVDF-4, and Au–NYCTO/PVDF-5 samples, respectively.

2.4 Characterization and dielectric measurement

The phase structures of NYCTO and Au–NYCTO particles were examined using X-ray diffractometry (XRD, PANalytical, EMPYREAN). Surface morphologies of Au, NYCTO and Au–NYCTO particles were revealed using transmission electron microscopy (TEM, FEI Tecnai G2 20). The fractured microstructure of the composites was observed using scanning electron microscopy (SEM, SEC, SNE-4500M). The crystalline phase of nanocomposites was determined using Fourier transform infrared spectroscopy (FTIR, Bruker, TENSOR27) in the wavenumber range of 600–1300 cm^{-1}. Thermal behavior and crystallinity of Au–NYCTO/PVDF composites were studied using a differential scanning calorimetry (DSC, PerkinElmer, 8000 Advanced Double-Furnace) with a heating rate of 20 °C min^{-1} under nitrogen atmosphere. Dielectric measurements of all samples were recorded using an impedance analyzer (KEYSIGHT E4990A) over the frequency range from 10^2 to 10^6 Hz. The temperature dependence of the dielectric properties was determined over the range of −60 °C to 150 °C. The oscillation voltage was 0.5 volts. The sample electrodes were silver coated on both surfaces of samples before dielectric measurements.

3. Results and discussion

The XRD patterns of the Au standard data, NYCTO, and Au–NYCTO powders are illustrated in Fig. 1. Comparing the XRD

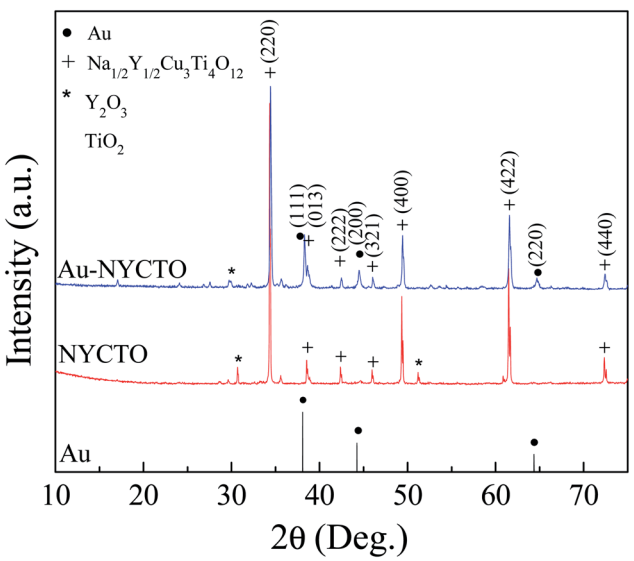

Fig. 1 XRD patterns of Au standard data, NYCTO and Au–NYCTO particles.

Open Access Article. Published on 06 November 2020. Downloaded on 12/5/2025 4:44:41 AM.
This article is licensed under a Creative Commons Attribution-NonCommercial 3.0 Unported Licence.

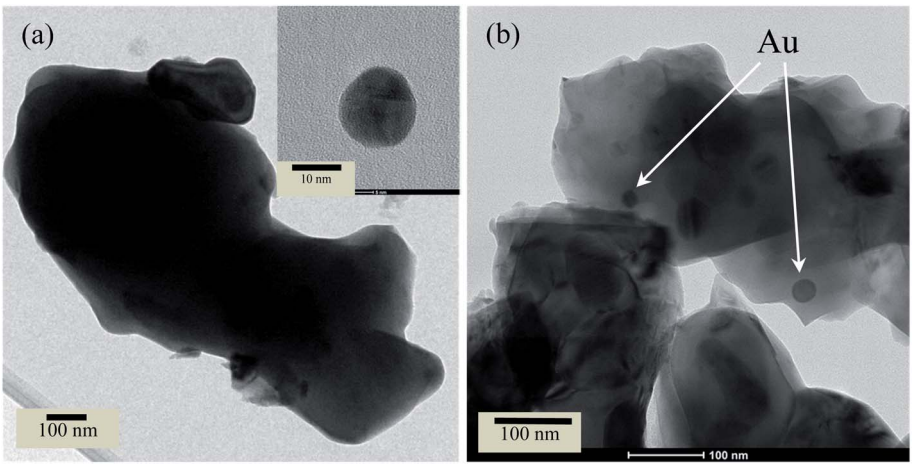

Fig. 2 TEM images of surface morphologies of (a) NYCTO, (b) Au–NYCTO particles. Inset of (a) shows a Au nanoparticle.

peak intensities of the NYCTO and Au–NYCTO powders, three additional diffraction peaks were observed in the XRD pattern of the Au–NYCTO powder, corresponding to the standard data of Au (JCPDS 00-001-1172). These peaks corresponded to the (111), (200) and (220) planes. The dominant peaks of (220), (013), (222), (321), (400), (422), and (440) planes were observed in the XRD patterns of the NYCTO and Au–NYCTO, corresponding to the perovskite-like NYCTO crystalline structure. However, small amounts of Y_2O_3 and TiO_2 phases were also detected.

The morphologies of the NYCTO particles and Au–NYCTO hybrid particles are shown in Fig. 2. The inset of Fig. 2(a) shows the morphologies of a Au nanoparticle. As revealed in Fig. 2(a), it can be seen that NYCTO displays an irregular shape. Meanwhile, the Au nanoparticle has a spherical shape that is ≈10 nm in diameter. Fig. 2(b) presents the distribution of Au nanoparticles on the surfaces of NYCTO particles. Au nanoparticles were discretely attached onto NYCTO surfaces. As reported by Luo *et al.*,[6] the discrete growth of Ag nanoparticles on $BaTiO_3$ particles can cause an increase in the dielectric response of the Ag–$BaTiO_3$/PVDF composites while suppressing increases in conductivity and dielectric losses. Similarly, enhanced dielectric performance is expected in the Au–NYCTO/PVDF composites.

Fig. 3 shows XRD patterns of Au–NYCTO/PVDF nanocomposites with various loadings of Au–NYCTO filler. All composites exhibit the evident peaks of NYCTO. The dominant peaks did not change in the composites with different filler loadings. The small characteristic peaks of Au were observed in the Au–NYCTO/PVDF composites. It is notable that the concentration of Au was ≈7.3 wt% in the Au–NYCTO hybrid particles. In the XRD patterns of the Au–NYCTO/PVDF composites, the α-PVDF phase was almost invisible since the semi-crystalline phase of PVDF decreased with the increased crystalline phase of Au–NYCTO. However, small amounts of impurity phases were still detected in the composites.

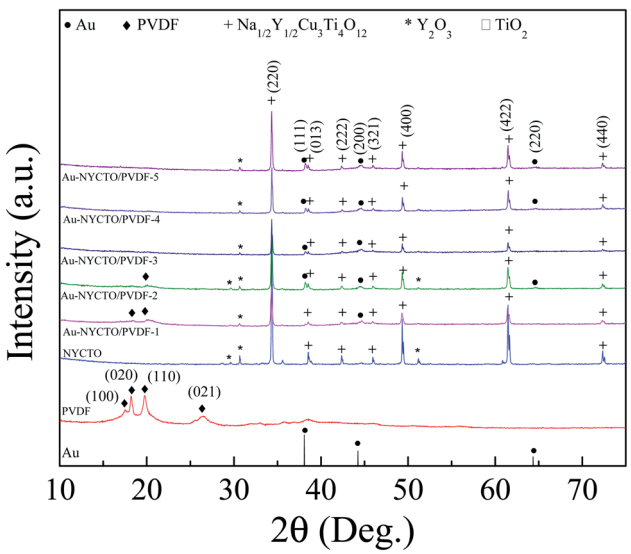

Fig. 3 XRD patterns of Au standard data, NYCTO particles and Au–NYCTO/PVDF nanocomposites with various contents of Au–NYCTO.

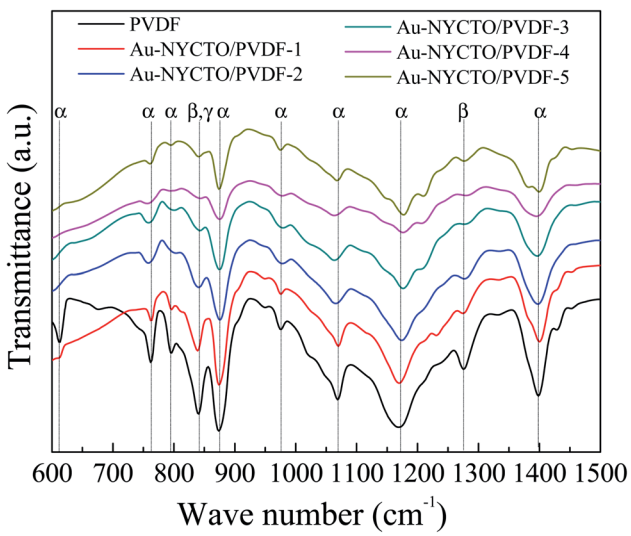

Fig. 4 FTIR spectra of nanocomposites with various contents of Au–NYCTO.

This journal is © The Royal Society of Chemistry 2020

Open Access Article. Published on 06 November 2020. Downloaded on 12/5/2025 4:44:41 AM.
This article is licensed under a Creative Commons Attribution-NonCommercial 3.0 Unported Licence.

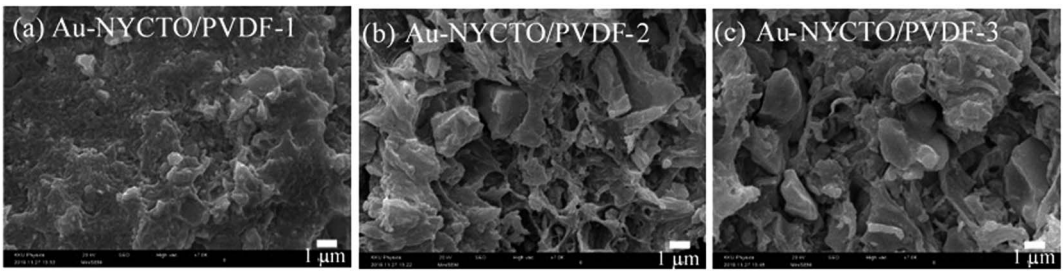

Fig. 5 SEM images of fractured morphologies of (a) Au–NYCTO/PVDF-1, (b) Au–NYCTO/PVDF-2, and (c) Au–NYCTO/PVDF-3 composites.

Fig. 4 presents the FTIR spectra of the Au–NYCTO/PVDF composites with various volume fractions of Au–NYCTO hybrid particles ($f_{Au-NYCTO}$). Characteristic transmittance peaks were observed, corresponding to the α-, β- and γ-phases of the PVDF polymer.[7,21] The characteristic bands of α-phase were observed at 613, 762, 797, 874, 976, 1071, 1177 and 1398 cm^{-1}.[22–24] The band at 841 cm^{-1}, assigned to the γ-phase.[22,23] At the same time appear bands at 841 and 1275 cm^{-1}, characteristic for β-phase.[22,23] Moreover, the bands at 613, 762, 874 and 1275 cm^{-1} were attributed to the CCC skeletal bending vibration. The characteristic bands at 874, 1071 and 1275 cm^{-1} were assigned to the CC skeletal symmetric stretching vibration, while the bands at 841, 874, 1177 and 1275 cm^{-1} were assigned to the CF_2 symmetric stretching vibration. The bending of CF_2 group was detected at 613 and 762 cm^{-1}. The wagging of CH_2 group was observed at 1398 cm^{-1}. The rocking of CH_2 and the twisting of CH_2 groups were detected at 841, 797 and 976, 1177 cm^{-1}, respectively. After Au–NYCTO hybrid particles were incorporated into the PVDF matrix, the transmittance intensity of the composites was reduced. The peaks of the α-, β- and γ-phases became weaker because of decreasing PVDF content. Notably, the β-PVDF phase was presented in the composites, which can result in enhancement of ε'.[25]

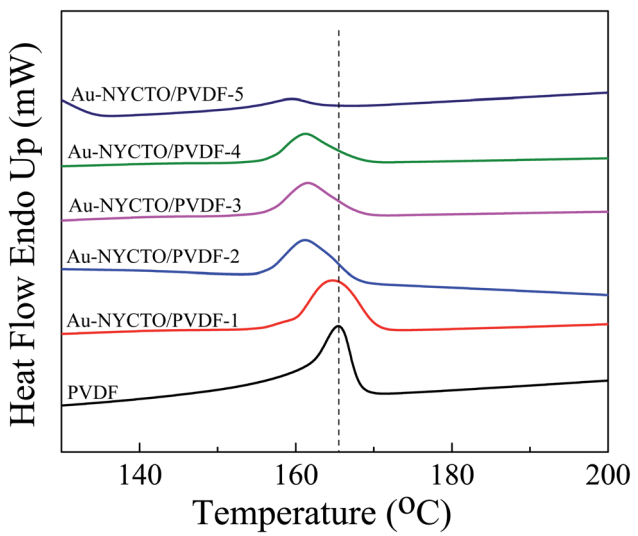

Fig. 6 DSC thermograph of Au–NYCTO/PVDF composites with various contents of Au–NYCTO.

Fig. 5 displays SEM images of the fractured cross-sections of Au–NYCTO/PVDF composites with various $f_{Au-NYCTO}$ fractions. As shown in Fig. 5(a), the PVDF matrix forms a continuous phase. The Au–NYCTO particles were homogenously and randomly dispersed due to a low $f_{Au-NYCTO}$. When $f_{Au-NYCTO}$ was increased to 0.191 and 0.289 [Fig. 5(b) and (c)] agglomeration of the filler was observed.

The DSC spectra of the Au–NYCTO/PVDF composites are shown in Fig. 6. The positions of the melting peaks (T_m) slightly shifted to a low temperature by incorporating Au–NYCTO. Besides, as the Au–NYCTO content increased, the enthalpy of melting (ΔH_m) and the crystallinity degree (X_c) of nanocomposites decreased obviously, as summarized in Table 1. The X_c of composites can be calculated by using the following equation $X_c = \frac{\Delta H_m}{\Delta H_{m100\%}} \times 100\%$, where ΔH_m is the melting enthalpy of the sample (J g^{-1}), and $\Delta H_{m100\%}$ is the melting enthalpy of fusion for 100% crystalline PVDF (104.7 J g^{-1}). It can be observed that the X_c decreased from 18.36% for a pure PVDF polymer to 2.06% for the composite with $f_{Au-NYCTO} = 0.487$. The result could be described that the Au–NYCTO particles hinder the PVDF polymer chain movement, affecting to the incomplete melting and crystallization process. This resulted in a further decrease in both the X_c and T_m.

The frequency dependence of ε' and tan δ at room temperature for the Au–NYCTO/PVDF composites with various f_{Au-}

Table 1 Melting temperature (T_m), melting enthalpy (ΔH_m), and crystallinity degree (X_c) of Au–NYCTO/PVDF composites with various contents of Au–NYCTO

Sample	Melting temperature, T_m (°C)	Melting enthalpy, ΔH_m (J g^{-1})	Crystallinity degree, X_c (%)
PVDF	165.54	19.22	18.36
Au–NYCTO/PVDF-1	164.75	18.91	18.06
Au–NYCTO/PVDF-2	161.27	17.65	16.86
Au–NYCTO/PVDF-3	161.58	14.65	13.99
Au–NYCTO/PVDF-4	161.23	11.68	11.16
Au–NYCTO/PVDF-5	159.43	2.16	2.06

Open Access Article. Published on 06 November 2020. Downloaded on 12/5/2025 4:44:41 AM.
This article is licensed under a Creative Commons Attribution-NonCommercial 3.0 Unported Licence.

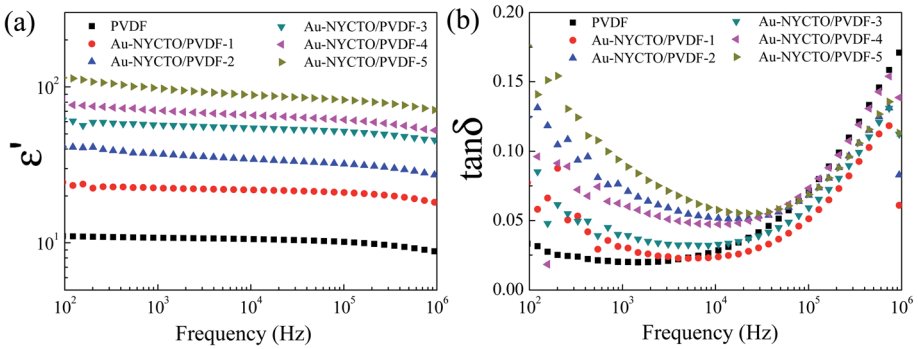

Fig. 7 Frequency dependence of (a) ε' and (b) tan δ at room temperature of Au–NYCTO composites with various contents of Au–NYCTO filler.

$_{NYCTO}$ fractions is shown in Fig. 7. ε' significantly increased with the $f_{Au-NYCTO}$ faction over the frequency range of 10^2 to 10^6 Hz. The ε' value of Au–NY/PVDF-5 ($f_{Au} = 0.075$, and $f_{NYCTO} = 0.412$) reached 97.9 at 1 kHz, which is ≈10 times higher than pure PVDF polymer. At 10^2 Hz, ε' was greater than 100. Furthermore, ε' of all composites was slightly dependent on the frequency over the measured frequency range. It is noteworthy that the tan δ values at 10^3 Hz of the composites were all lower than 0.1. This result is rarely observed in other ceramic/polymer composite systems.[10,26–32] Compared with two-phase NYCTO/PVDF composites ($\varepsilon' \sim 84$, tan $\delta \sim 0.11$ at 1 kHz) with $f_{NYCTO} = 0.5$, a higher ε' value (~98) for the three-phase Au–NYCTO/PVDF composite with $f_{Au-NYCTO} = 0.487$ was achieved with a lower tan δ, ~0.09. This demonstrates that surface decoration of NYCTO with Au nanoparticles should result in increased dielectric response. Fang *et al.*[33] reported a greatly enhanced $\varepsilon' \sim 208$ at 1 kHz in the BT–(31 wt%)Ag/PVDF composite with $f_{BT-Ag} = 0.563$, while tan δ was very large (0.155). It was also reported that a high $\varepsilon' \sim 320$ at 1 kHz with high tan $\delta \sim 0.2$ was obtained in ($f = 0.2$)BT–($f = 0.2$)Ni/PVDF composite.[34] It is important to note that the ε' value of the Au–NYCTO/PVDF composite with $f_{Au-NYCTO} = 0.487$ was lower than those of the BT–Ag/PVDF and BT–Ni/PVDF composites. This may be due to the weakened δ-phase (polar phase) in composites.

Obviously, incorporation of small amounts of Au nanoparticles into the composite system can promote interfacial polarization, giving rise to the increased dielectric response. In other words, the increased conductivity of the interlayer between NYCTO and PVDF created by Au nanoparticles enhances the Maxwell–Wagner–Sillars (MWS) effect.[35] tan δ shows a different tendency in low- and high-frequency ranges, as seen in Fig. 7(b). The tan δ values in the low-frequency range from 10^2 to 10^5 Hz are greatly increased with $f_{Au-NYCTO}$ due to interfacial polarization, which is obviously weakened with increased frequency. A sharp increase tan δ is noted at frequencies over 10^5 Hz, which is a typical feature of the glass transition relaxation of the PVDF matrix.[10] In a high-frequency range, tan δ slightly decreased with increasing $f_{Au-NYCTO}$. It noteworthy that the enhanced ε' of the Au–NYCTO/PVDF composites was significantly increased, while largely increased tan δ was suppressed. ε' and tan δ values at 10^3 and 10^4 Hz (at room temperature) of the Au–NYCTO/PVDF composites with various filler loadings are given in Table 2.

The temperature dependence of ε' and tan δ for the Au–NYCTO composites with various $f_{Au-NYCTO}$ fractions are illustrated in Fig. 8. The ε' value increased with temperature. Generally, in a low-temperature range, the dipoles freeze and become resistant to rotation caused by the applied electric field.[36,37] At higher temperatures, the dipoles can easily be rotated by an applied electric field. Hence, polarization can be fully produced, giving rise to obtain a larger ε'. It was observed that ε' rapidly increased at temperatures higher than 100 °C, corresponding to greatly increased tan δ values. This result can be attributed to interfacial polarization associated with the conduction of free charge carriers in the composites.[6] A tan δ relaxation peak was observed in the temperature range from −50 to 0 °C, Fig. 8(b). This relaxation was attributed to the glass transition temperature of the PVDF polymer.[38,39]

Fig. 9 shows variations of ε' and tan δ for composites as a function of $f_{Au-NYCTO}$ at room temperature and 1 kHz. ε' of the Au–NYCTO/PVDF composites continuously and linearly increased with the content of Au–NYCTO. The significant increase in ε' of the Au–NYCTO/PVDF can be ascribed to the homogeneous dispersion of Au–NYCTO in the PVDF polymer. Surprisingly, tan δ was kept to values lower than 0.1 for all composites—no abrupt changes in ε' and tan δ at any $f_{Au-NYCTO}$ level was observed. Therefore, no percolation network or concurrent conducting pathways were formed in the composites with $f_{Au-NYCTO} \leq 0.487$.[40,41] Thus, the percolation theory (PT) cannot be used to explain the dielectric behavior of the Au–NYCTO/PVDF composites. This may be due to the fact that the maximum loading of Au nanoparticles in the composites is 7.5 vol%, while the theoretical percolation threshold (f_c) of an

Table 2 Volume fraction (f) of each component, ε' and tan δ at 1 kHz and 10 kHz of Au–NYCTO/PVDF nanocomposites

				1 kHz		10 kHz	
Sample	f_{Au}	f_{NYCTO}	$f_{Au-NYCTO}$	ε'	tan δ	ε'	tan δ
PVDF	0	0	0	10.8	0.020	10.6	0.028
Au–NYCTO/PVDF-1	0.008	0.087	0.095	22.5	0.030	21.9	0.023
Au–NYCTO/PVDF-2	0.019	0.172	0.191	37.3	0.073	34.4	0.051
Au–NYCTO/PVDF-3	0.032	0.257	0.289	51.2	0.040	54.7	0.033
Au–NYCTO/PVDF-4	0.049	0.338	0.387	70.8	0.061	66.1	0.047
Au–NYCTO/PVDF-5	0.075	0.412	0.487	97.9	0.090	89.0	0.068

This journal is © The Royal Society of Chemistry 2020

Open Access Article. Published on 06 November 2020. Downloaded on 12/5/2025 4:44:41 AM.
This article is licensed under a Creative Commons Attribution-NonCommercial 3.0 Unported Licence.

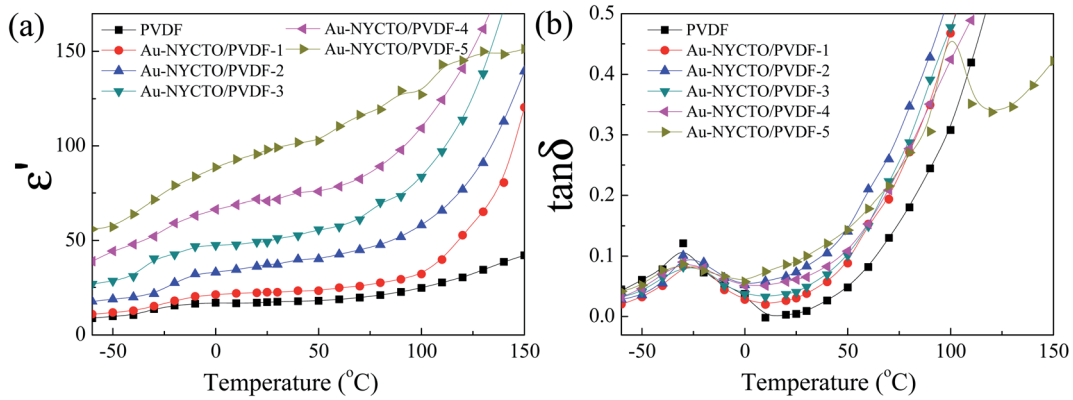

Fig. 8 Temperature dependence of (a) ε', and (b) tan δ at 10^3 Hz of Au–NYCTO/PVDF composites with various contents of Au–NYCTO composite.

insulator-matrix composites filled with the spherical conductor-nanoparticles is ~16 vol% ($f_c = 0.16$).[40,41] Basically, the effective medium theory (EMT), Maxwell–Garnett (M–G), Yamada, and Lichtenecker models cannot be used to describe the dielectric behavior of the Au–NYCTO/PVDF composites because these models were derived without considering the interfacial effect between the filler and matrix.

Alternatively, a combination of the PT and EMT models, *i.e.*, the effective medium percolation theory model (EMPT), may be more suitable than either model alone.[27,42] The EMPT model is usually used to predict the ε' value of ceramic–metal/polymer composites (*e.g.*, $BaTiO_3$–Cu/PVDF composites).[43] The effective dielectric permittivity (ε_{eff}) of the composites can be expressed as eqn (1),

$$\varepsilon_{eff} = \varepsilon_{PVDF}\left[1 + \frac{f_{Au-NYCTO}(\varepsilon_{Au-NYCTO} - \varepsilon_{PVDF})}{\varepsilon_{PVDF} + n(1 - f_{Au-NYCTO})(\varepsilon_{Au-NYCTO} - \varepsilon_{PVDF})}\right] \left|\frac{f_c - f_{Au-NYCTO}}{f_c}\right|^{-q}, \quad (1)$$

where, $\varepsilon_{Au-NYCTO} \sim 6701$ and $\varepsilon_{PVDF} \sim 11$ are the experimental dielectric permittivities of the NYCTO and PVDF polymer matrix, respectively. n is the filler morphology fitting factor of a ceramic filler. f_c and q are the percolation threshold and a critical component, respectively. As demonstrated in Fig. 10, the filler volume-fraction dependence of ε' can be well described by the EMPT model. The calculated ε_{eff} values and the experimental ε' values are consistent. According to the fitted result, $f_c = 0.69$, $q = 0.1$, and $n = 0.13$. It is important to note that $n = 0.13$ is equal to $n = 0.13$ for the $Na_{0.5}Bi_{0.5}Cu_3Ti_4O_{12}$/PVDF composites,[10] and is comparable to $n = 0.11$ for the $CaCu_3Ti_4O_{12}$/PVDF composites.[26] As expected, the calculated f_c value of the Au–NYCTO/PVDF composites was higher than the maximum loading of Au–NYCTO filler with $f_{Au-NYCTO} = 0.487$. This composite contained 7.5 vol% Au nanoparticles ($f_{Au} = 0.075$), while the theoretical f_c values for the insulator matrix composites filled with metallic spherical nanoparticles is 16 vol% ($f_c = 0.16$).[40] Thus, the rapid change in ε' cannot be observed in the experimental result. The inset of Fig. 10 shows the correlation between f_{Au} and $f_{Au-NYCTO}$. According to the exponential fitted curve, the correlation can be expressed as eqn (2),

$$f_{Au} = 0.008 \exp(4.609 f_{Au-NYCTO}). \quad (2)$$

By taking $f_{Au-NYCTO} = 0.69 = f_c$, f_{Au} can be roughly calculated using eqn (2) and obtained to be 0.19. Interestingly, $f_{Au} = 0.19$ is consistent with the theoretical f_c value (0.16). Therefore, it can be confirmed that the achieved excellent dielectric properties of the Au–NYCTO filler with $f_{Au-NYCTO} = 0.487$ should not be associated with the percolation effect.

When the volume fraction of Au–NYCTO hybrid particles increased to 0.487, the high-permittivity NYCTO loading and Au nanoparticles increased. Thus, the first reason for the increased dielectric response in the composite was attributed to a very high ε' of the NYCTO filler particles. The ε' and tan δ values at 1 kHz of the two-phase NYCTO/PVDF composite with $f_{NYCTO} = 0.4$ was found to be ~66 and 0.099, respectively. The ε' value of the three-phase composite with $f_{Au-NYCTO} = 0.487$ (*i.e.*, $f_{Au} = 0.075$ and $f_{NYCTO} = 0.412$) was ~98. The ε' of the NYCTO/PVDF composite with $f_{NYCTO} = 0.4$ can be increased by ~48% after the addition of 7 vol% Au nanoparticles. The second reason for the enhanced ε' of the Au–NYCTO/PVDF composite was

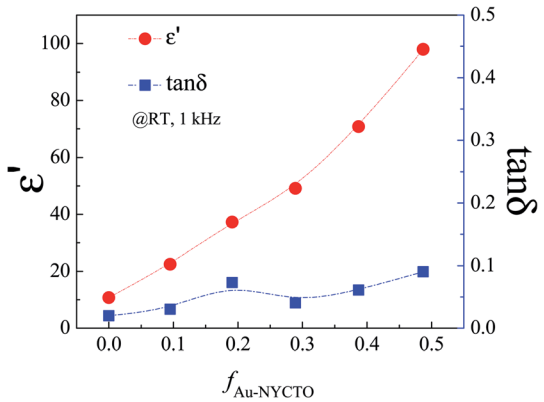

Fig. 9 ε' and tan δ at room temperature and 10^3 Hz for Au–NYCTO/PVDF composites with various contents of Au–NYCTO.

Open Access Article. Published on 06 November 2020. Downloaded on 12/5/2025 4:44:41 AM.
This article is licensed under a Creative Commons Attribution-NonCommercial 3.0 Unported Licence.

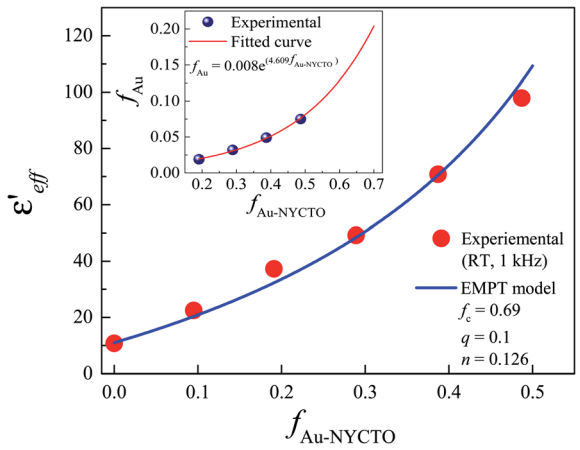

Fig. 10 ε' (1 kHz) of Au–NYCTO/PVDF composites fitted by EMPT model. Inset shows the correlation of f_{Au} and $f_{Au-NYCTO}$; the solid curve is the best exponential fitting data.

attributed to the increase in the interfacial polarization intensity. Furthermore, the interparticle distance between the Au–NYCTO hybrid particles would be shortened as $f_{Au-NYCTO}$ increased. The effect of micro–capacitor formation was dominant as the dielectric layer (*i.e.*, β-PVDF) between two inner electrodes (*i.e.*, Au nanoparticles) was thinner, giving rise to the enhanced capacitance value of the micro–capacitor. Notably, tan δ values of the NYCTO/PVDF and Au–NYCTO/PVDF composites were nearly the same in value. Thus, the incorporation of Au nanoparticles has a slight effect on the dielectric loss. This may be due to the discrete growth of Au nanoparticles on the surface of NYCTO particles, preventing the direct contact between Au nanoparticles.[6,44–46] It is worth noting that the dielectric properties of the Au–NYCTO/PVDF composites could be further improved by adjusting the Au concentration in the hybrid particles. A higher dielectric response may be achieved by increasing the Au concentration in the hybrid particles due to the increased interfacial polarization.

4. Conclusions

PVDF polymer composites incorporating Au–NYCTO hybrid particles were successfully fabricated. Au nanoparticles were decorated on the NYCTO surfaces using a modified Turkevich's method. The polar β-PVDF phase was detected in the composites, which has an important contribution to the enhanced dielectric response. The weakened δ-phase in composites inhibited a largely enhanced ε' value. The ε' value at 10^3 Hz of the composite with $f_{Au-NYCTO} = 0.487$ was obtained 97.9, while tan δ was 0.09. According to fitted data using the EMPT model, the percolation behavior was predicted to exist at $f_{Au-NYCTO} = 0.69$ ($f_{Au} \sim 0.19$), corresponding to $f_c = 0.16$ for the theoretical value of the conductor–insulator composites. A largely enhanced ε' in the Au–NYCTO/PVDF composites was associated with the interfacial polarization effect and a high ε' of the NYCTO ceramic filler. The introduction of Au nanoparticles produced stronger interfacial polarization.

Conflicts of interest

There are no conflicts to declare.

Acknowledgements

This work was financially supported by the Synchrotron Light Research Institute, Khon Kaen University, and the Thailand Research Fund (TRF) [Grant No. BRG6180003]. It was partially supported by the Research Network NANOTEC (RNN) program of the National Nanotechnology Center (NANOTEC), NSTDA, Ministry of Higher Education, Science, Research, and Innovation (MHESI) and the Research Program of Khon Kaen University, Thailand. N. P. would like to thank the Graduate School, Khon Kaen University for partially support with a partial scholarship under the Post-doctoral Program (60170), Thailand. P. K. would like to thank the Science Achievement Scholarship of Thailand (SAST) for her PhD of Science Degree scholarship.

References

1 Z. M. Dang, Y. H. Lin and C. W. Nan, *Adv. Mater.*, 2003, **15**, 1625–1629.
2 Z.-M. Dang, H.-Y. Wang, Y.-H. Zhang and J.-Q. Qi, *Macromol. Rapid Commun.*, 2005, **26**, 1185–1189.
3 Z.-M. Dang, T. Zhou, S.-H. Yao, J.-K. Yuan, J.-W. Zha, H.-T. Song, J.-Y. Li, Q. Chen, W.-T. Yang and J. Bai, *Adv. Mater.*, 2009, **21**, 2077–2082.
4 W. Zhou, L. Xu, L. Jiang, J. Peng, Y. Gong, X. Liu, H. Cai, G. Wang and Q. Chen, *J. Alloys Compd.*, 2017, **710**, 47–56.
5 Z.-M. Dang, Y.-F. Yu, H.-P. Xu and J. Bai, *Compos. Sci. Technol.*, 2008, **68**, 171–177.
6 S. Luo, S. Yu, R. Sun and C.-P. Wong, *ACS Appl. Mater. Interfaces*, 2014, **6**, 176–182.
7 P. Martins, A. C. Lopes and S. Lanceros-Mendez, *Prog. Polym. Sci.*, 2014, **39**, 683–706.
8 M.-F. Lin, V. K. Thakur, E. J. Tan and P. S. Lee, *RSC Adv.*, 2011, **1**, 576–578.
9 X. Zhang, S. Zhao, F. Wang, Y. Ma, L. Wang, D. Chen, C. Zhao and W. Yang, *Appl. Surf. Sci.*, 2017, **403**, 71–79.
10 Y.-l. Su, C. Sun, W.-q. Zhang and H. Huang, *J. Mater. Sci.*, 2013, **48**, 8147–8152.
11 P. Thomas, R. S. E. Ravindran and K. B. R. Varma, *Polym. Eng. Sci.*, 2014, **54**, 551–558.
12 C. Yang, H.-s. Song and D.-b. Liu, *Composites, Part B*, 2013, **50**, 180–186.
13 P. Liang, Y. Li, Y. Zhao, L. Wei and Z. Yang, *J. Appl. Phys.*, 2013, **113**, 224102.
14 W. Somphan, N. Sangwong, T. Yamwong and P. Thongbai, *J. Mater. Sci.: Mater. Electron.*, 2011, **23**, 1229–1234.
15 J. Jumpatam, A. Mooltang, B. Putasaeng, P. Kidkhunthod, N. Chanlek, P. Thongbai and S. Maensiri, *Ceram. Int.*, 2016, **42**, 16287–16295.
16 Z. Wang, W. Zhou, L. Dong, X. Sui, H. Cai, J. Zuo and Q. Chen, *J. Alloys Compd.*, 2016, **682**, 738–745.
17 H. S. Ju, D. H. Im, S. D. Park, H. G. Lee and E. S. Kim, *Jpn. J. Appl. Phys.*, 2012, **51**, 09ML01.

This journal is © The Royal Society of Chemistry 2020

Open Access Article. Published on 06 November 2020. Downloaded on 12/5/2025 4:44:41 AM.
This article is licensed under a Creative Commons Attribution-NonCommercial 3.0 Unported Licence.

18 X. Huang, P. Jiang and L. Xie, *Appl. Phys. Lett.*, 2009, **95**, 242901.
19 J. Audoit, L. Laffont, A. Lonjon, E. Dantras and C. Lacabanne, *Polymer*, 2015, **78**, 104–110.
20 S. Luo, S. Yu, R. Sun and C. P. Wong, *ACS Appl. Mater. Interfaces*, 2014, **6**, 176–182.
21 N. Meng, X. Zhu, R. Mao, M. J. Reece and E. Bilotti, *J. Mater. Chem. C*, 2017, **5**, 3296–3305.
22 Y. Bormashenko, R. Pogreb, O. Stanevsky and E. Bormashenko, *Polym. Test.*, 2004, **23**, 791–796.
23 H.-C. Yang, Q.-Y. Wu, H.-Q. Liang, L.-S. Wan and Z.-K. Xu, *J. Polym. Sci., Part B: Polym. Phys.*, 2013, **51**, 1438–1447.
24 S. Lanceros-Méndez, J. F. Mano, A. M. Costa and V. H. Schmidt, *J. Macromol. Sci., Part B: Phys.*, 2001, **40**, 517–527.
25 J. Yao, C. Xiong, L. Dong, C. Chen, Y. Lei, L. Chen, R. Li, Q. Zhu and X. Liu, *J. Mater. Chem.*, 2009, **19**, 2817–2821.
26 P. Thomas, K. T. Varughese, K. Dwarakanath and K. B. R. Varma, *Compos. Sci. Technol.*, 2010, **70**, 539–545.
27 K. Meeporn, P. Thongbai, T. Yamwong and S. Maensiri, *RSC Adv.*, 2017, **7**, 17128–17136.
28 Z.-M. Dang, H.-P. Xu, D. Xie and L. Li, *Mater. Lett.*, 2007, **61**, 511–515.
29 P. Kum-onsa, P. Thongbai, S. Maensiri and P. Chindaprasirt, *J. Mater. Sci.: Mater. Electron.*, 2016, **27**, 9650–9655.
30 D. Bhadra, A. Biswas, S. Sarkar, B. K. Chaudhuri, K. F. Tseng and H. D. Yang, *J. Appl. Phys.*, 2010, **107**, 124115.
31 K. Meeporn, S. Maensiri and P. Thongbai, *Appl. Surf. Sci.*, 2016, **380**, 67–72.
32 M. Fang, Z. Wang, H. Li and Y. Wen, *Ceram. Int.*, 2015, **41**(suppl. 1), S387–S392.
33 F. Fang, W. Yang, S. Yu, S. Luo and R. Sun, *Appl. Phys. Lett.*, 2014, **104**, 132909.
34 Z.-M. Dang, Y. Shen and C.-W. Nan, *Appl. Phys. Lett.*, 2002, **81**, 4814–4816.
35 C. Zhang, Q. Chi, J. Dong, Y. Cui, X. Wang, L. Liu and Q. Lei, *Sci. Rep.*, 2016, **6**, 33508.
36 C. C. Homes, T. Vogt, S. M. Shapiro, S. Wakimoto and A. P. Ramirez, *Science*, 2001, **293**, 673–676.
37 J. Wu, C.-W. Nan, Y. Lin and Y. Deng, *Phys. Rev. Lett.*, 2002, **89**, 217601.
38 A. C. Lopes, C. M. Costa, R. S. i. Serra, I. C. Neves, J. L. G. Ribelles and S. Lanceros-Méndez, *Solid State Ionics*, 2013, **235**, 42–50.
39 T. Zhou, J.-W. Zha, R.-Y. Cui, B.-H. Fan, J.-K. Yuan and Z.-M. Dang, *ACS Appl. Mater. Interfaces*, 2011, **3**, 2184–2188.
40 C. W. Nan, Y. Shen and J. Ma, *Annu. Rev. Mater. Res.*, 2010, **40**, 131–151.
41 C.-W. Nan, *Prog. Mater. Sci.*, 1993, **37**, 1–116.
42 K. Meeporn, N. Chanlek and P. Thongbai, *RSC Adv.*, 2020, **10**, 2747–2756.
43 C. Li, S. Yu, S. Luo, W. Yang, Z. Ge, H. Huang, R. Sun and C.-P. Wong, *RSC Adv.*, 2016, **6**, 36450–36458.
44 N. Phromviyo, N. Chanlek, P. Thongbai and S. Maensiri, *Appl. Surf. Sci.*, 2018, **446**, 59–65.
45 N. Phromviyo, P. Thongbai and S. Maensiri, *Appl. Surf. Sci.*, 2018, **446**, 236–242.
46 P. Kum-onsa, N. Chanlek, B. Putasaeng and P. Thongbai, *Ceram. Int.*, 2020, **46**, 17272–17279.